

Table 1 Impeller wheel geometries

Wheel No.	r_{1h} mm	r_{1t} mm	r_2 mm	β_{1tbl} deg	β_{2bl} deg	b_2 mm
A	16.0	36.8	63.5	59	-40	6.0
B	16.0	36.8	63.5	59	-40	5.5

Table 2 Diffuser geometries

Diffuser No.	A_4	r_3/r_2	r_5/r_2	LWR	2θ deg	AR
S19112	1025	1.1	1.57	3.75	12	1.79
B74850	850	1.1	1.57	5.26	9	1.83

Experimental and theoretical analysis of centrifugal compressor impeller flow

H KRAIN, Dr-Ing

German Aerospace Research Establishment (DFVLR), Cologne, West Germany

ABSTRACT

The results of extensive laser measurements carried out in a 30 deg. back-swept, medium pressure ratio impeller ($\pi_t = 4.7:1$) are used for quantitative comparisons between measured and calculated data. The L2F-measurement technique available at DFVLR has been used to analyze the flow field inside the rotating flow passages of the impeller. The quasi-3-D calculation method used to prepare the theoretical data is part of an impeller design procedure developed at DFVLR. Predominantly good agreement between measurement and calculation is obtained in the inducer part of the impeller, whereas noticeable deviations in flow angles and through flow velocities are found in the shroud/exit area. A detailed analysis of the actual flow reveals a distinct vortex development in the areas of maximum differences between measured and calculated data. The vortex flow initiates cross-flows and distorted through flow patterns that are not taken into account by the quasi-3-D approach.

NOMENCLATURE

B	= stream sheet thickness (hub-to-shroud)
b	= stream sheet thickness (blade-to-blade)
c_L	= absolute velocity measured with L2F-velocimeter
$c_m L$	= meridional velocity derived from laser measurements
c_ϕ	= circumferential vortex velocity (Fig.12)
$h_{t,rel}$	= rothalpy
\vec{n}	= mass flow rate
	= normal unit vector of the stream surface
n/n_0	= shaft speed referred to the design shaft speed
p_S	= pressure side
p_R	= static pressure
r_f	= gas constant
z	= cylindrical coordinates
θ	= radius of solid-body vortex
s	= suction side
T	= entropy
u_2	= temperature (K)
	= impeller tip speed

\vec{w}	= relative velocity vector
y/t	= dimensionless blade pitch
z/b	= dimensionless channel depth
β_L	= relative flow angle measured by L2F-velocimeter
η_{Ptt12}	= total/total polytropic impeller efficiency
η_{Stt14}	= total/total isentropic stage efficiency
ν	= kinematic viscosity
π_{t12}	= total pressure ratio of the rotor
π_{t14}	= total stage pressure ratio
ρ	= density
ψ	= stream function
ω	= angular velocity

INTRODUCTION

Today the quasi-three-dimensional stream sheet approach is a widely used calculation method for practical centrifugal compressor design [1,2,3,4,5]. This approach - originally introduced by Wu [6] - simplifies the prediction of a 3-D flow-field by introducing two types of stream surfaces, thus reducing the physical 3-D flow to an idealized flow problem that can be numerically treated in a two dimensional way [7]. The velocity vectors are assumed to be tangential to the stream surfaces which excludes a mass flow transportation through the stream surfaces. An additional assumption is, that the fully 3-D flow can be predicted by an iterative calculation procedure on both types of stream surfaces. However, in practice difficulties already arise when the first reasonable surface has to be defined. For example, if the flow field of a centrifugal impeller has to be predicted, then it is not easy to decide which surface suits the flow development best. Usually, the calculation starts on a mean hub-to-shroud surface located at mid-pitch in the flow channel. Towards the impeller exit, however, this surface generally deviates from the mid-pitch position thus taking care of slip effects. This procedure is equivalent to the assumption that the flow is almost blade-congruent and that there are no secondary flows in the pitchwise direction. In a next step the flow properties are generally calculated on axi-symmetric blade-to-blade surfaces thus excluding secondary flows from hub-to-shroud.

From measurements it is well known that there are very often significant secondary flows inside centrifugal impeller rotors that violate the assumptions implied in the quasi-3-D approach [8,9,10]. Therefore, differences between the predicted and actual flow field are to be expected in the areas of increased secondary flows. But frequently users of quasi-3-D calculation methods cannot assess the differences to be expected which in general is due to a lack of experimental data.

This paper gives some information about the problem indicated. A comparison between measured and calculated data carried out for a 30 deg. backswept medium pressure ratio impeller will show that noticeable differences between measured and calculated cross-flow and through-flow patterns are presumably due to the channel vortices contained in the flow field.

RESEARCH COMPRESSOR AND MEASUREMENT TECHNIQUE

A 30 deg. backswept impeller designed and manufactured at DFVLR [2,3] has been used for the experimental and theoretical research work (Fig.1). For the initial tests this impeller was coupled with a vaneless diffuser of constant area which ensured a wide flow range. The impeller was designed for a mass flow rate of 4.0 kg/s and a rotor pressure ratio of 4.7:1.

For performance measurements total temperatures as well as total pressures have been measured at the compressor inlet and exit. Additionally, the static pressure development has been measured along the shroud contour from rotor inlet to the diffuser exit. The total pressure ratio of the rotor and the rotor efficiency were deduced from static pressure measurements (24 tappings) at the rotor discharge and by using the equations of energy and continuity. For these calculations a zero blockage has been assumed at the rotor exit.

Fig.2 shows the measured performance map of the centrifugal compressor stage. Maximum achieved stage pressure ratio was 4.5:1, maximum achieved stage efficiency was 84%. A relatively wide flow range of about 36% has been measured for 100% shaft speed which is primarily due to the vaneless diffuser used for these tests. Fig.3 shows the rotor performance map. Maximum rotor pressure ratio for 105% shaft speed was 5.5:1, maximum achieved isentropic impeller efficiency was 94%.

The internal flow field of the rotor was analyzed with the L2F-measurement technique available at DFVLR [11,12]. Six measurement planes have been selected to analyze the 3-D flow with the laser measurement technique. The position of the laser measurement planes is indicated in Fig.4 and their distinct location is submitted in Table 1. All measurement planes are perpendicular to the impeller shroud contour. Basically the L2F-tech-

nique is a two dimensional measurement technique, but if the laser beam is oriented almost perpendicular to the main flow direction, a fully 3-D flow field can be analyzed.

Table 1

Measurement plane	Location x/s m
I	0
II	0.2
III	0.4
IV	0.6
V	0.8
VI	1.004

The measurement technique applied gives information about the magnitude and direction of the mean absolute velocity vector and about its turbulent components. The relative velocity vector is easily derived from the velocity triangle. The estimated error for the mean velocity measurement generally is less than $\pm 1\%$, the error in absolute flow angle measurements usually is less than ± 1 deg. [12].

THEORETICAL APPROACH

The test results obtained for the new backswept rotor were used to check the reliability and applicability of the impeller design procedure developed at DFVLR [2]. A block diagram illustrating the design approach is submitted in Fig.5. Initially, the impeller geometry is generated and the geometrical data necessary for the fluid dynamic calculation are prepared. The quasi-3-D flow field calculation applied is based on Wu's stream sheet approach [6,13]. The calculation starts on a mean hub-to-shroud surface and is continued on axisymmetric blade-to-blade surfaces which can be chosen for different radial positions. The input data for the blade-to-blade solutions are taken from the hub-to-shroud solution and from the programme preparing the geometrical input data (programme GEOB). Thus the results of the blade-to-blade solutions are directly dependent on the hub-to-shroud solution, but a reaction of the blade-to-blade solutions on the hub-to-shroud solution is neglected. Finally, boundary layer calculations are carried out at all boundaries [14]. The results obtained by the design procedure can be analyzed with the plot modules PLOT1:PLOT indicated in Fig.5. For the comparison of measured and calculated data the theoretical results obtained with the hub-to-shroud solutions and with the blade-to-blade solutions have been used. The basic equations to be solved for this quasi-3-D approach are:

$$\text{Continuity: } \nabla \cdot (\rho \vec{w}) = 0$$

$$\text{Momentum: } -\vec{w}_x(\vec{\nabla} \times \vec{w}) + 2\vec{w} \times \vec{w} = -\vec{\nabla} h_{t,\text{rel}} + T \vec{v}_s$$

$$\text{Energy (no preswirl): } \vec{\nabla} h_{t,\text{rel}} = 0$$

$$\text{State of gas: } \rho/\rho_0 = (T/T_0)^{1/(k-1)} \cdot e^{-(s-s_0)/R}$$

$$\text{Geometric conditions: } \vec{n} \cdot \vec{w} = 0$$

Equations (2) and (4) are indicating that an entropy distribution is taken into account during the solution procedure. This distribution is derived by assuming a constant static/static polytropic impeller efficiency that has to be chosen according to experience. An impeller inlet flow without preswirl is assumed. From equation (3) it is seen that the rothalpy is assumed constant throughout the impeller. This assumption simplifies the numerical solution procedure. However, it is not a necessity. Equation (5) describes the assumption that the relative flow vector \vec{w} is a tangent to the stream surface introduced. The geometry of the stream surface is described by the normal unit vector \vec{n} . Introducing a stream function, ψ , into equations (1-5) results in two nonlinear partial differential equations of second order that have to be numerically solved to obtain the blade-to-blade and hub-to-shroud solutions:

Blade-to-Blade Calculation:

$$\begin{aligned} A(z, \Theta) \frac{\partial^2 \psi}{\partial z^2} + B(z, \Theta) \frac{\partial^2 \psi}{\partial z \partial \Theta} + C(z, \Theta) \frac{\partial^2 \psi}{\partial \Theta^2} \\ + D(z, \Theta, \rho, b) \frac{\partial \psi}{\partial z} \\ + E(z, \Theta, \rho, b) \frac{\partial \psi}{\partial \Theta} + F(z, \Theta, \rho, b, \omega, s, \partial \psi / \partial \Theta) = 0 \end{aligned} \quad (6)$$

Hub-to-Shroud-Calculation:

$$\begin{aligned} A(r, z) \frac{\partial^2 \psi}{\partial r^2} + B(r, z) \frac{\partial^2 \psi}{\partial r \partial z} + C(r, z) \frac{\partial^2 \psi}{\partial z^2} + D(r, z, \rho, B) \frac{\partial \psi}{\partial r} \\ + E(r, z, \rho, B) \frac{\partial \psi}{\partial z} + F(r, z, \rho, B, \omega, s, \partial \psi / \partial r) = 0 \end{aligned} \quad (7)$$

The coefficients A-F in equations (6) and (7) are primarily dependent on the stream surface geometry, on density, entropy and angular velocity. A derivation of equations (1-7), details about the numerical procedure applied and information about the boundary conditions used for a centrifugal impeller are given in ref. [7].

COMPARISON BETWEEN MEASUREMENT AND CALCULATION

Figs.6-11 are illustrating the results of a detailed comparison between measured and calculated data carried out for the rotor design point ($\dot{m}=4 \text{ kg/s}$, $n/n_0=1$, Fig.3). Measured and calculated meridional velocities as well as relative flow angles are plotted for the six laser measurement planes shown in Fig.4. For each plane the comparison has been carried out at five different channel depths ($z/b=0.1 \dots z/b=0.9$). The measured and calculated data are plotted against the dimensionless blade pitch y/t . The pressure side of the blade is located at the left, the suction side is located at the right. The calculated data are interpolated data taken from 10 blade-to-blade calculations carried out at 10 z/b -positions that slightly differed from the laser z/b -positions which are plotted in Figs.6-11.

Fig.6 shows the comparison between measured and calculated data at plane I. A good agreement is obtained for the meridional velocities from the shroud ($z/b=0.1$) to the hub ($z/b=0.9$). The relative flow angles are in good agreement from the shroud ($z/b=0.1$) to the middle of the flow channel ($z/b=0.5$), whereas noticeable deviations are present close to the hub. This is due to the thick leading edges in this area that displace the actual flow, whereas the boundary conditions used for the calculation are assuming an almost blade congruous flow in this area. This condition has been taken from experience, i.e. laser-measurements carried out in the inlet area of radially ending impellers revealed a blade congruous flow just aft of the impeller leading edge [2,10,15]. Fig.7 illustrates the comparison between measured and calculated data for measurement plane II. A throughout good agreement is obtained for the meridional velocities as well as for the relative flow angles. Similarly, a predominantly good agreement is also obtained for plane III (Fig.8). Noticeable deviations between measured and calculated data are only present close to the shroud. In this area the actual meridional velocities are found to be lower than the calculated whereas the flow angles are slightly higher. Continuity of the actual flow is obviously conserved by slightly higher meridional velocities in the hub area. Surprising results, that are not easily explained, were obtained for measurement plane IV (Fig.9). At this measurement position significant differences between measured and calculated data are present from the shroud ($z/b=0.1$) up to the middle of the flow channel ($z/b=0.5$). Flow angle differences greater than 20 deg. are present close to the shroud ($z/b=0.1 \dots 0.2$). Here the measured meridional velocity profiles are also significantly disturbed. In the shroud area the actual meridional velocities are lower than the calculated ones whereas this tendency is reversed in the hub area. This was to be expected since both the actual and the calculated flow fields have to satisfy continuity. Thus, a reasonable agreement between measured and calculated meridional velocities is only obtained for the integral flow field whereas significant deviations are locally found.

Similar tendencies as in plane IV are present in plane V (Fig.10). Here again significant differences between measured and calculated flow angles are analyzed in the shroud region. In this area the measured meridional velocities are also significantly differing from the calculated ones.

Fig.11 shows the comparison between measured and calculated data for measurement plane VI. Here a slightly better agreement than in planes IV and V is obtained for the flow angles. At the blade surface the calculated flow angles coincide with the blade design angle ($\beta_L = 60 \text{ deg.}, 30 \text{ deg. backswept}$), whereas the flow angles are less than 60 deg. inside

of the flow channel ($0 < y/t < 1$) which is due to the slip effects taken into account. The measured meridional velocities are again locally deviating from the calculated data.

In summary, a predominantly good agreement between measured and calculated data is obtained for measurement planes I, II and III. However, significant differences in flow angles and meridional velocities are observed in the shroud area of measurement planes IV, V and VI. Primarily the measured flow angle distributions reveal strong secondary flows that are not taken into account by the calculation procedure. Obviously the differences between the measured and calculated meridional velocities are also maximum in those areas where the flow angle differences are maximum indicating an interdependence between the through flow pattern and the secondary flow pattern. The interrelationship of these phenomena can be best explained by studying the vortex flow of the impeller.

Basically the L2F-technique is a two dimensional measurement technique. A light gate is created by two discrete light beams and the velocity component perpendicular to the laser beam axis is derived from the time a particle needs to pass the gate [11]. The velocity component parallel to the laser beam axis cannot be measured with this measurement technique.

Therefore, a direct measurement of a vortex flow is not possible with the L2F-technique since such an approach necessitates a 3-D-measurement technique. However, the existence of a vortex can be proved indirectly by using the L2F-measurement results.

VORTEX FLOW

Information about the vortex flow inside the flow passages of centrifugal compressor rotors can be extracted from the lines of constant relative flow angles (isoclines). The structure of the isocline pattern plotted from the measured laser data reveal whether a distinct vortex is present in the actual flow or not. The basic relations for the isoclines of a real vortex measured with the L2F-measurement technique have been derived by Binder [16,17]. The equations submitted in Fig.12 are valid for an idealized vortex assumed to be composed of a solid-body-vortex part ($0 \leq r \leq r_0$, Fig.12) and of a potential vortex part ($r_0 < r$). Any real vortex will have a similar structure. The velocity distribution $c_\phi = c_\phi(r)$ of such a vortex is shown in Fig.12. The L2F-velocimeter can only measure the velocity component perpendicular to the laser beam axis ($c_{\phi L}$). Within the flow channel the blade congruous relative velocity w_b is superimposing the circumferential vortex velocity c_ϕ . From the velocity triangle it can be derived that the L2F-velocimeter will measure the relative flow angle β_L of such a flow. Therefore it can easily be derived from the velocity

triangle that lines of $\beta_L = \text{konst.}$ are described by the following simple equations (Fig.12):

$$y = \text{konst.} \quad 0 \leq r \leq r_0 \quad (8)$$

$$\begin{aligned} y/r^2 &= \text{konst.} \\ x &= \pm \sqrt{r^2 - y^2} \\ x &= \pm \frac{\sqrt{r^2 - y^2}}{\sin \beta_b} \quad r_0 < r \end{aligned} \quad (9)$$

The result of that analysis is submitted in Fig.13 indicating that the isoclines are parallel to each other in the solid body vortex area whereas these lines exhibit an elliptical shape in the potential vortex area. The vortex center is located in the middle of the parallel isoclines. The idea presented is used to identify vortices contained in the impeller flow, i.e. isoclines are plotted from the L2F-measurement results and a real vortex, composed of a solid-body and potential vortex part, is assumed to be present when an isocline pattern similar to that shown in Fig.13 is analyzed.

Figs.14-16 are showing the isoclines of the backswept impeller plotted for measurement planes IV to VI (Fig.4). The isocline patterns are exhibiting all features typical of real vortices. Two counterrotating channel vortices are clearly identified in measurement plane IV and V, whereas only one channel vortex could be identified from the isocline plot of plane VI. Significant differences in the relative flow angles and parallel isoclines have also been analyzed close to the shroud of measurement planes IV to VI. However, a clearly developed vortex, as in the middle of the flow channel, has not been resolved in this area. The isocline pattern is suggesting that only a solid-body-vortex part is present in this area which seems to be due to the relative motion between the moving blades and the stationary casing. A comparison with Figs.9-11 reveals that maximum differences between the measured and calculated velocities and between measured and calculated flow angles are observed in those areas where the vortices have been analyzed. The vortices, of course, are generating cross-flows in the pitchwise as well as in the hub-to-shroud direction that are not taken into account by the quasi-3D approach. The differences between the actual and calculated relative flow angles are easily explained by this model.

The differences in calculated and measured meridional velocities are also supposed to be due to the vortex development. From experience and theory it is well known that the through flow velocity component of a swirling flow is reduced in the vortex center [18,19,20]. Fig.17 illustrates this effect for three vortices. A vortex flow with a zero radial velocity component ($w_r = 0$) and an axial velocity component varying only in the radial direction is assumed

$(w_z = w_z(r))$. For these assumptions the following relations can be derived from the Navier-Stokes equations:

$$\frac{w_\phi^2}{r} = \frac{1}{\rho} \frac{\partial p}{\partial r} \quad (10)$$

$$p(\phi) = \text{konst.} \quad (11)$$

$$\nu \frac{1}{r} \frac{\partial}{\partial r} \left(r \frac{\partial w_z}{\partial r} \right) = 0 \quad (12)$$

A relation for the through flow velocity distribution in a real vortex can easily be derived by integrating equation (12). The result of this approach is shown in Fig.17. The through flow velocity has a maximum at the edge of the vortex ($r/r_{\max} = 1$) and is decreasing towards the center of the vortex. The descent depends on the radius ratio r_{\max}/r_0 that relates the potential vortex part to the solid-body vortex part of the overall vortex. The shape of these curves qualitatively agrees with the measurement results obtained in the shroud area of the impeller at measurement planes IV to VI (Figs.9-11). Here, the through flow velocity is also decreasing in the areas of the vortex centers. Obviously the distorted actual through flow patterns deviating from the predicted patterns are also due to the vortex development inside of the flow passages.

REFERENCES

- [1] Casey, M.V.: "The Aerodynamic Development of High-Performance Radial Compressor Stages for Industrial Turbocompressors". VDI Bericht 572.1, pp.167-181.
- [2] Krain, H.: "A CAD Method for Centrifugal Compressor Impellers". ASME Journal of Engineering for Gas Turbines and Power, Vol.106, April 1984, pp.482-488.
- [3] Krain, H.; Rogge, H.: "Design and Manufacturing of High Pressure Ratio Centrifugal Compressor Impellers". VDI Bericht 572.1, pp.437-460 (in German).
- [4] Harada, H.: "Performance Characteristics of Two- and Three-Dimensional Impellers in Centrifugal Compressors". ASME-Paper 86-GT-154, p.6.
- [5] Japikse, D.; Osborne, C.: "Optimization of Industrial Centrifugal Compressors". ASME-Paper 86-GT-221, p.14.
- [6] Wu, C.H.: "A General Theory of Three-Dimensional Flow in Subsonic and Supersonic Turbomachines of Axial, Radial and Mixed-Flow Types". NACA TN-2604, 1952, p.92.
- [7] Krain, H.: "Contribution to the Quasi-Three-Dimensional Calculation within Centrifugal Compressor Impellers". Doctoral thesis, Technische Hochschule Aachen, Dec. 1975, p.185 (in German).

- [8] Hamkins, C.P.; Flack, R.D.: "Laser Velocimeter Measurements in Shrouded and Unshrouded Radial Flow Pump Impellers". ASME-Paper 86-GT-129, p.7.
- [9] Krain, H.: "A Study on Centrifugal Impeller and Diffuser Flow". ASME Journal of Engineering for Power, Vol.103, No.4, Oct. 1981, pp.688-697.
- [10] Eckardt, D.; Krain, H.: "Secondary Flow Studies in High-Speed Centrifugal Compressor Impellers". AGARD-CP-214, 18.1-18.13.
- [11] Schodl, R.: "A Laser-Two-Focus (L2F) Velocimeter for Automatic Flow Vector Measurements in the Rotating Components of Turbomachines". ASME-Paper 1980, in "Measurement Methods in Rotating Components of Turbomachinery", pp.139-147.
- [12] Schodl, R.: "Optical Technique for Turbomachinery Flow Analysis". Nato Institute, Izmir 1984.
- [13] Wu, C.H.: "Matrix Solution of Compressible Flow on S_1 Surface Through a Turbomachine Blade Row with Splitter Vanes or Tandem Blades". ASME-Paper 83-GT-10, p.8.
- [14] Bradshaw, P.; Unsworth, K.: "An Improved Fortran Program for the Bradshaw-Ferris-Atwell Method of Calculating Turbulent Shear Layers". I.C. Aero Report 74-02, Feb. 1974, p.51.
- [15] Eckardt, D.: "Detailed Flow Investigations within a High-Speed Centrifugal Compressor Impeller". Journal of Fluids Engineering, TRANS.ASME, Sept. 1976, pp.390-402.
- [16] Binder, A.: "Instationary Flow Effects in the Rotor of a Turbine". Thesis, University of Aachen, DFVLR-FB 85-66, p.157 (in German).
- [17] Binder, A.; Förster, W.; Mach, K.; Rogge, H.: "Unsteady Flow Interaction Caused by Stator Secondary Vortices in a Turbine Rotor". ASME-Paper 86-GT-302, p.8.
- [18] Meldau, E.: "Drallströmung im Drehhohlraum". Thesis Univ. of Hannover, 1935 (in German).
- [19] Acrivellellis, M.: "Untersuchungen an turbulenten Drallströmungen hinter einem radialen Leitapparat". Thesis, Univ. of Karlsruhe, 1974 (in German).
- [20] Neuberger, W.: "Calculation of Compressible Swirling Flows in Pipes, Annuli and on Rotating Cylinders". DFVLR-FB 80-21, p.107 (in German).

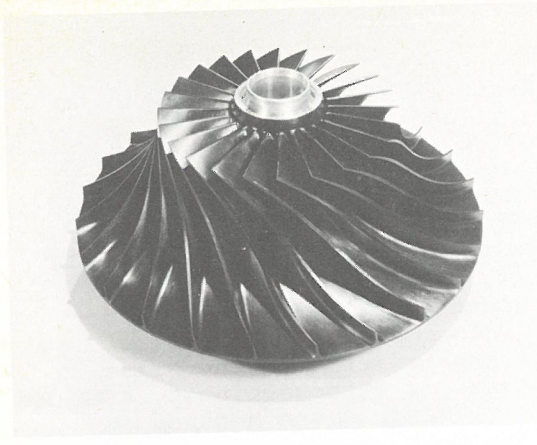


Fig 1 Thirty degree backswept impeller, $\dot{m} = 4.0 \text{ kg/s}$,
 $\pi_{t12} = 4.7:1$

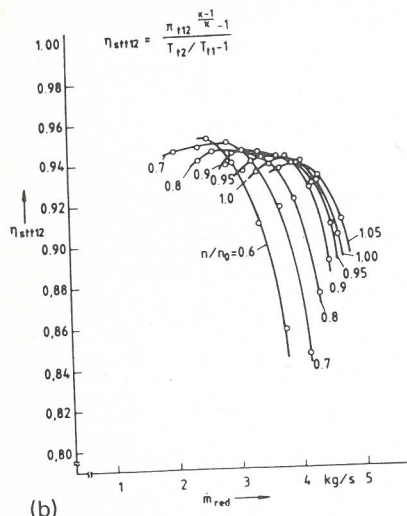
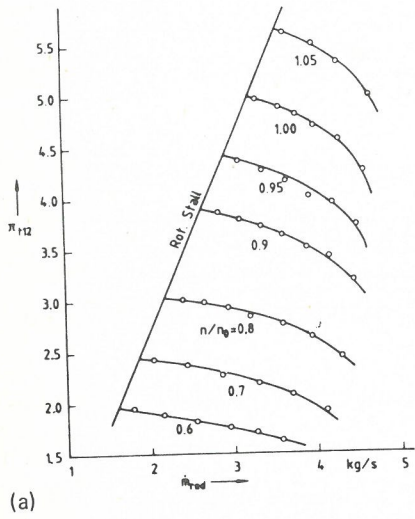


Fig 3 Rotor performance map

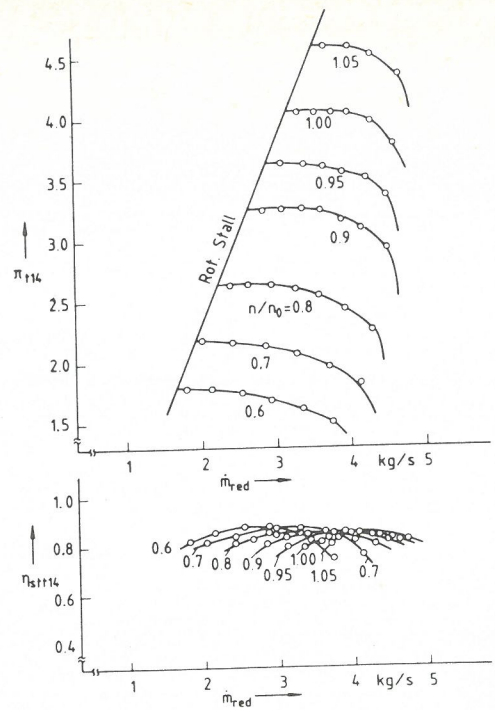


Fig 2 Performance map of the compressor, equipped with the backswung impeller and a vaneless diffuser

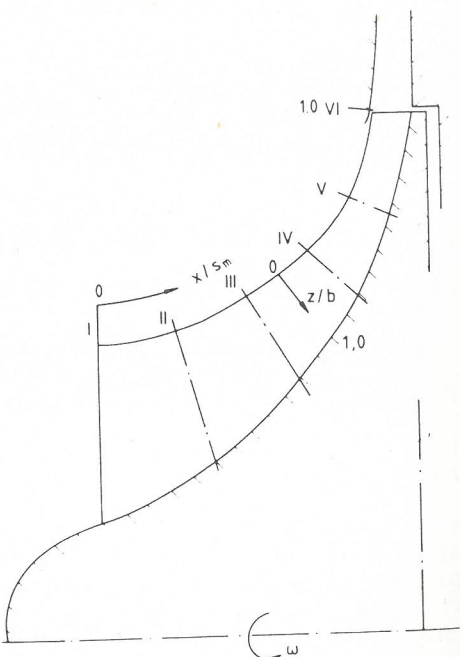


Fig 4 Location of L2F-measurement planes in the rotor area (Table 1)

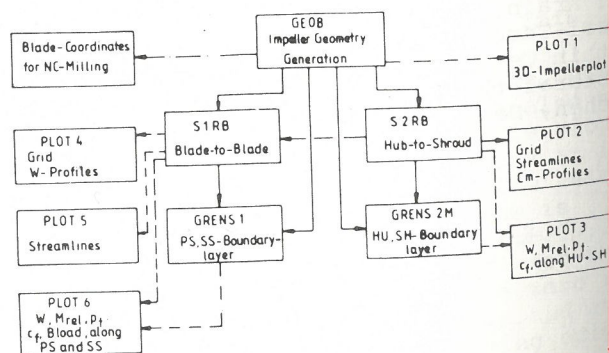


Fig 5 Block diagram of the impeller design package

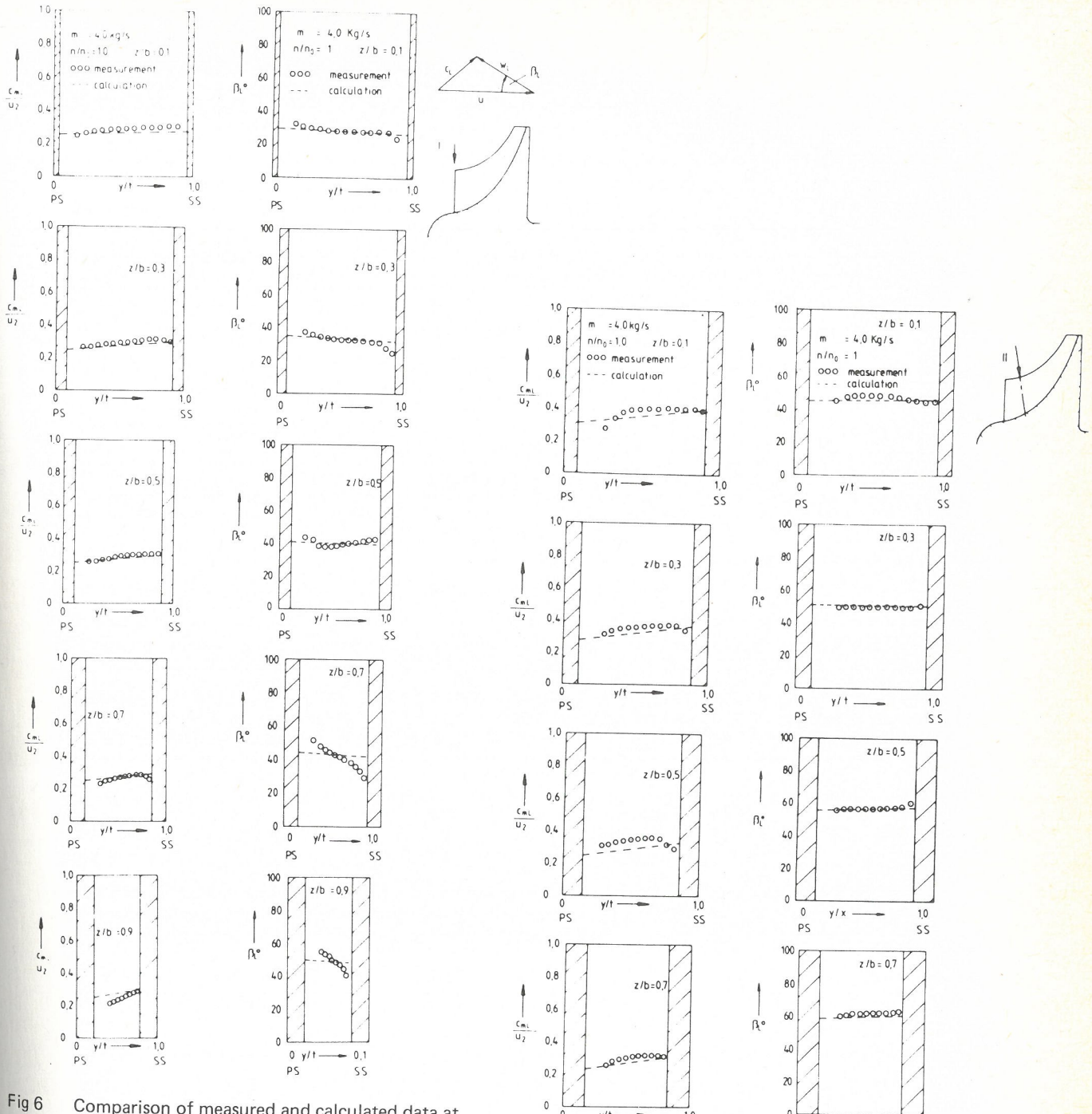


Fig 6 Comparison of measured and calculated data at plane I

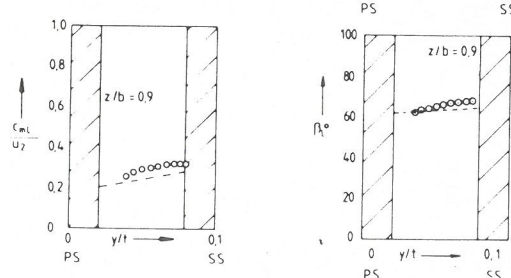


Fig 7 Comparison of measured and calculated data at plane II

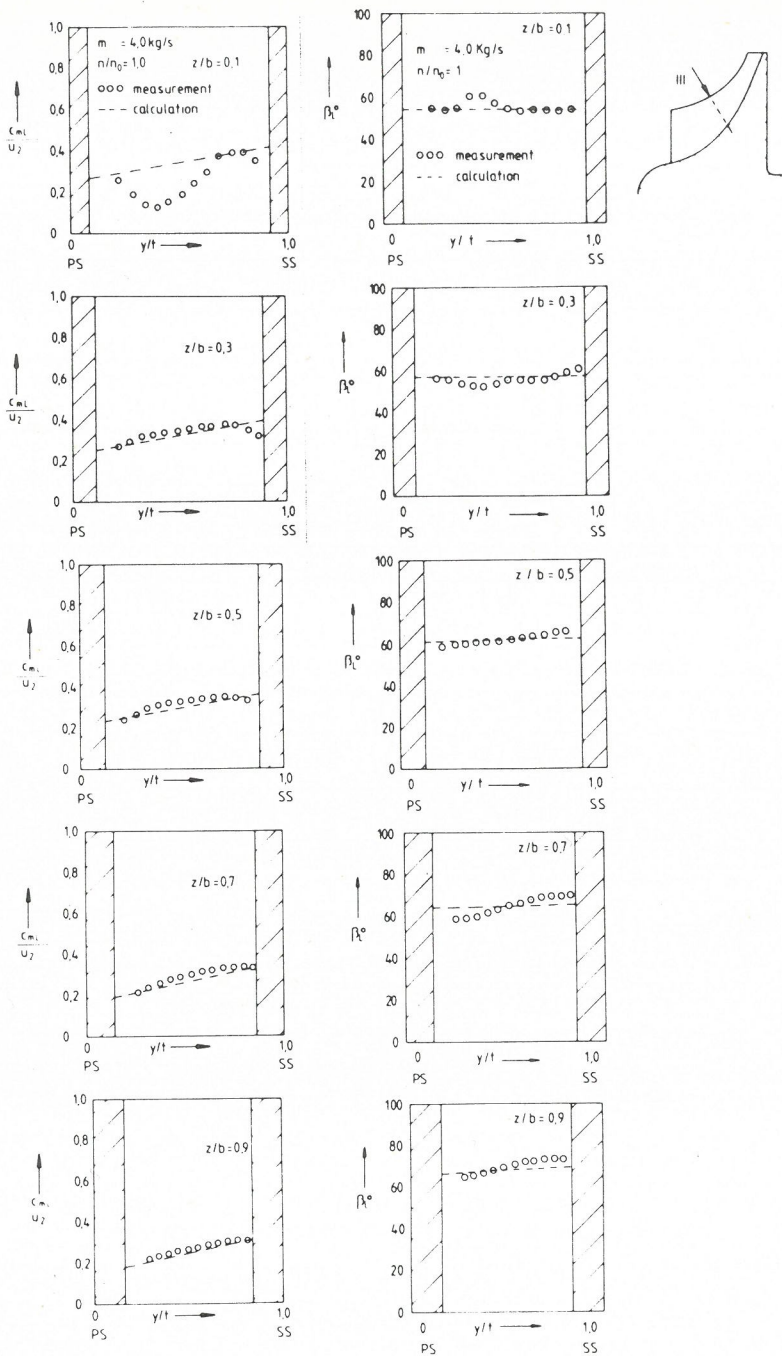


Fig 8 Comparison of measured and calculated data at plane III

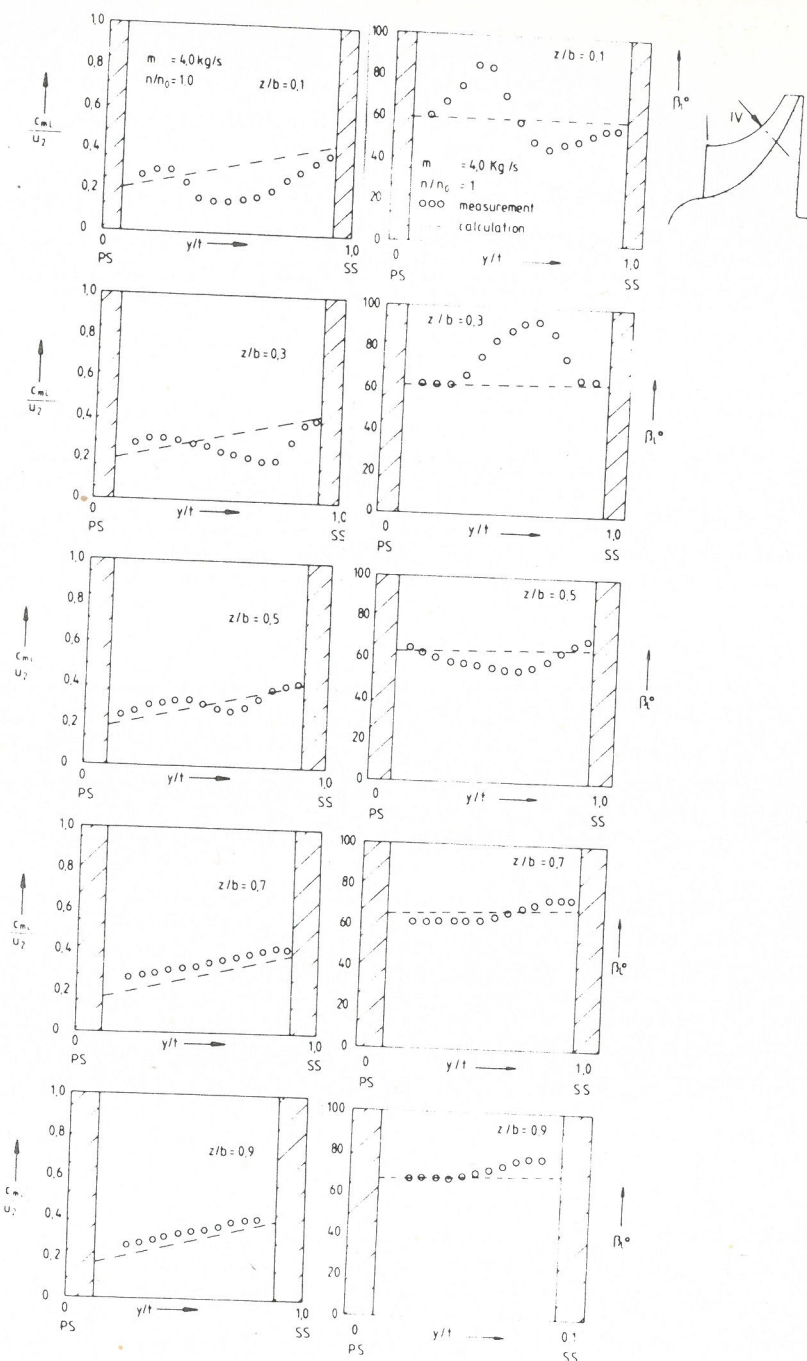


Fig 9 Comparison of measured and calculated data at plane IV

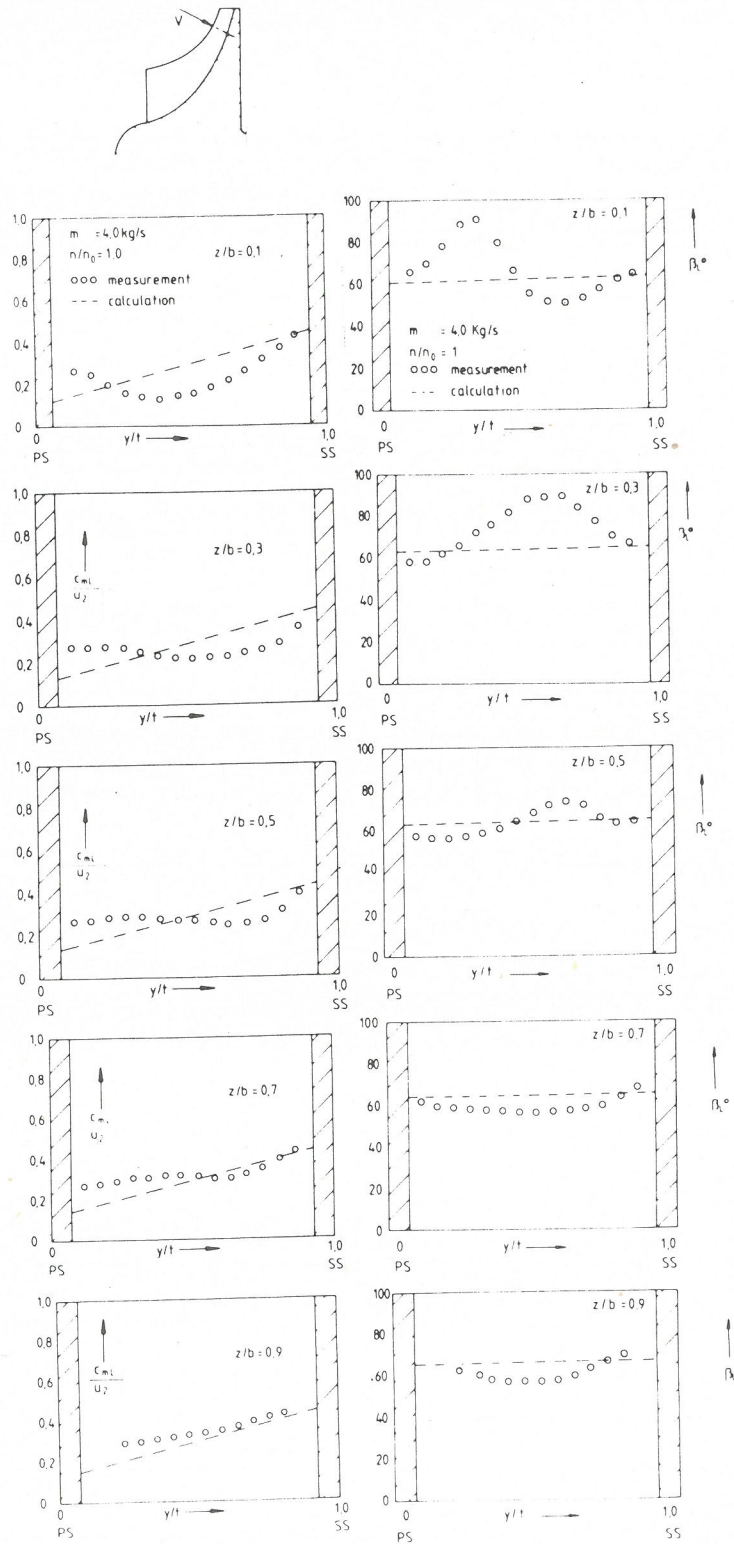


Fig 10 Comparison of measured and calculated data at plane V

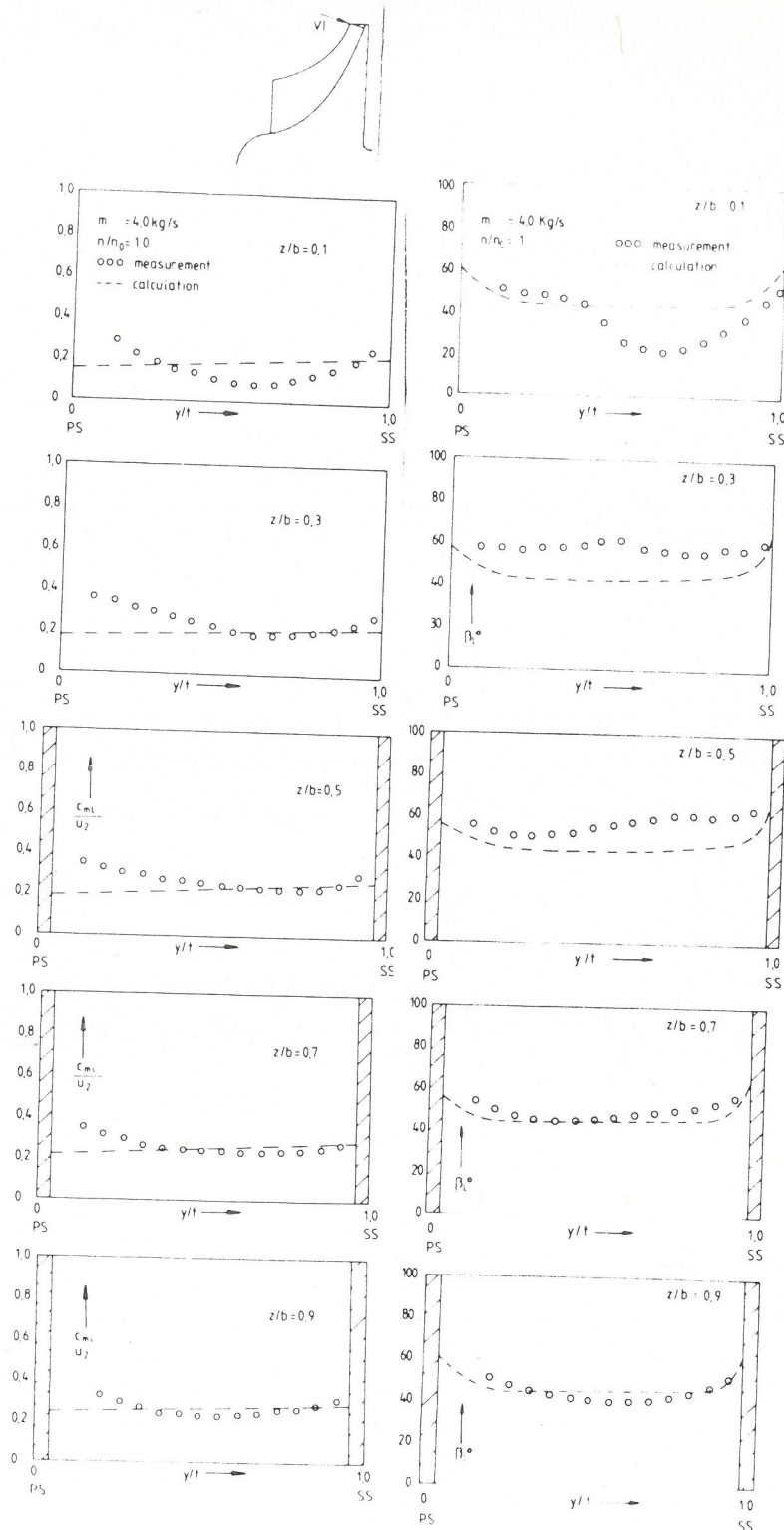


Fig 11 Comparison of measured and calculated data at plane VI

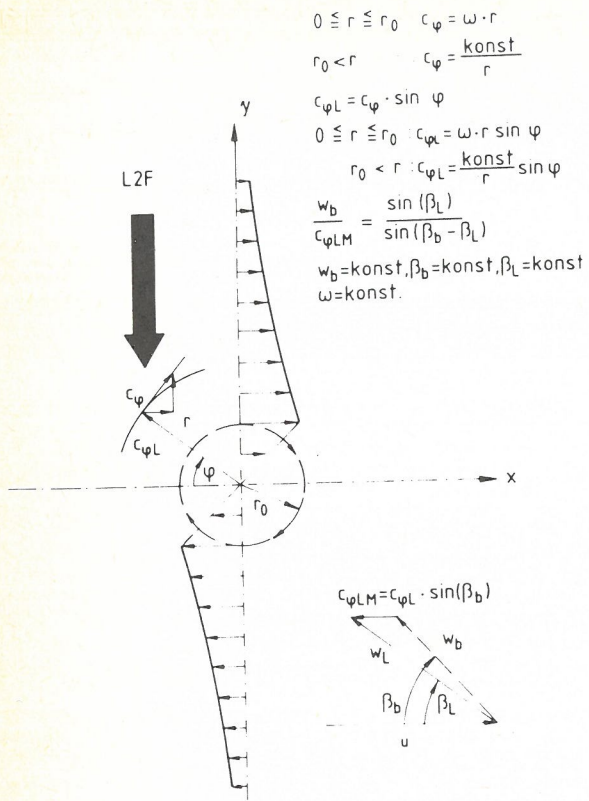


Fig 12 Measurement of vortex flow with L2F-measurement technique

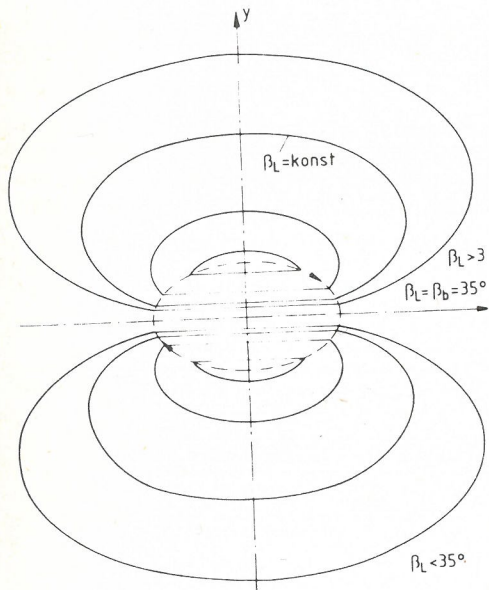


Fig 13 Isocline structure for a real vortex, composed of a solid body and a potential vortex part

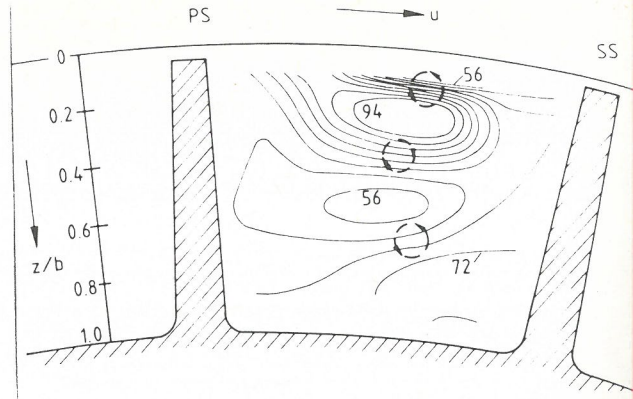


Fig 14 Isocline pattern ($\beta_L = \text{constant}$) measured at plane IV ($n/n_0 = 1$, $m_{\text{red}} = 4.0 \text{ kg/s}$)

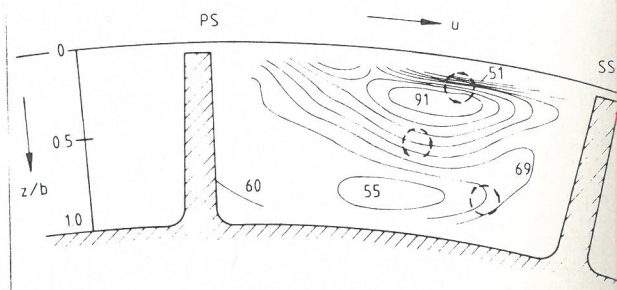


Fig 15 Isocline pattern ($\beta_L = \text{constant}$) measured at plane V ($n/n_0 = 1$, $m_{\text{red}} = 4.0 \text{ kg/s}$)

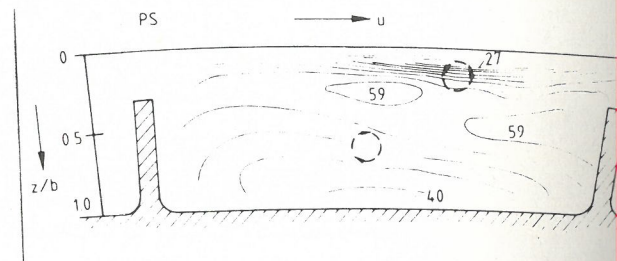


Fig 16 Isocline pattern ($\beta_L = \text{constant}$) measured at plane VI ($n/n_0 = 1$, $m_{\text{red}} = 4.0 \text{ kg/s}$)

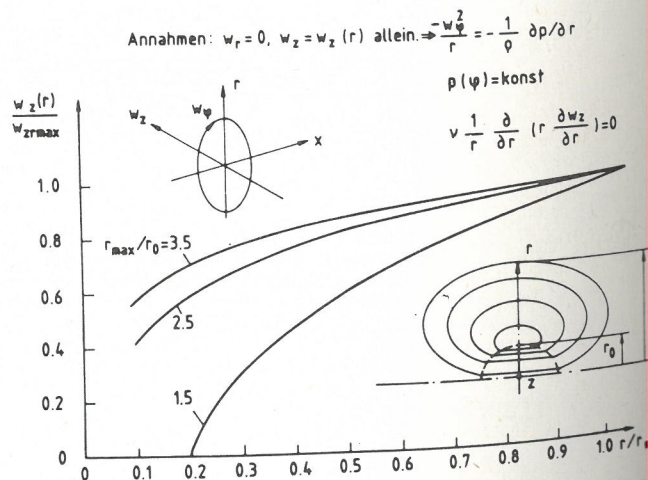


Fig 17 Through flow velocity distribution in a vortex

Laser doppler anemometer measurements and flow predictions in a turbine nozzle cascade

G D WILLIS, BTech, CEng, MIMechE

NEI-APE Limited W H Allen, Bedford

A GOULAS, Dipl Eng, MSc, DIC, PhD

Department of Mechanical Engineering, Cranfield Institute of Technology, Bedford

SYNOPSIS

Measurements of velocities in an air cascade, Reynolds number 220 000, were taken using a laser doppler anemometer. The air cascade was a model of a steam turbine nozzle (stator blade) row. The main objective of the experiment was to produce two-dimensional cascade flow to take measurements on blade-to-blade stream surfaces, to validate a computer model of the flow. The mapping showed the flow to be two-dimensional in the centre of the cascade and free from secondary flow effects. Velocity measurements in the centre plane confirmed the computer programme to predict the velocity distribution to within the experimental error.

1 INTRODUCTION

Laser doppler anemometry is an established tool for flow measurement. Applications include the study of secondary flow (1) and the verification of computer models of the flow in cascades (2, 3, 4). Many computer programmes to predict the flow in turbomachinery exist, such as the time marching solutions of Denton (5) and the through flow analysis of Bosman and Marsh(6). Recent review papers (7,8) discuss many of the computer programmes in use. The Fluid Engineering Unit, Cranfield Institute of Technology has developed a suite of turbomachinery flow analysis computer programmes (9, 10), based on Wu's general approach (11) and Marsh's matrix through flow solution (12). In collaboration with W.H.Allen the computer programmes have recently been adapted to analyse the flow in a low reaction axial flow turbine stator passage (13). The analysis programmes have been experimentally verified for their other applications but not for turbine stator passages.

The principal aim of the experimentation was to verify the two-dimensional analysis programme for low reaction axial flow turbine stator blade passages. Therefore it was necessary to produce two-dimensional flow on the centre plane of a cascade. The velocity distribution was measured using a laser doppler anemometer. To check if the flow was substantially two-dimensional, measurements were also taken at a quarter span and near to the end wall. A two beam laser doppler anemometer, as used, will only give the in-plane component of velocity, hence two components need to be taken to produce a two-dimensional map as it is impractical to align the laser with the flow direction throughout the domain. For simplicity the axial and tangential components were chosen.

2 THE COMPUTER ANALYSIS

The computer programme is a two-dimensional subsonic inviscid solution coupled with an

integral boundary layer calculation. The computer programme uses a finite difference scheme and solves for the stream function distribution in the blade passage. The R.A.E. method (14) is used to predict the boundary layer growth which is included in the analysis by a transpiration model to change the stream function boundary conditions for the inviscid flow. Usually, three to five inviscid-viscous interactions are required to produce a fully converged solution for a low reaction turbine stator passage.

It is possible to use the blade-to-blade (S1) solution in conjunction with a hub-to-shroud (S2) solution to give a quasi-three-dimensional solution. An S2 analysis of a typical turbine stator row showed there is little radial velocity component of the flow and it was therefore decided to use the S1 stream surface flow analysis on its own. For the cascade analysis the blades were set on a 10m radius which for practical purposes produced a linear cascade row. The computational mesh used 20 blade-to-blade stations and 100 axial stations, 40 of which were between the leading and trailing edge plane. The grid used uniform blade-to-blade spacing for each axial station and a grid ratio as close as practical to unity throughout the flow domain.

3 THE EXPERIMENTAL FACILITY

The cascade tunnel is part of W.H.Allen's experimental development facility. It is supplied with air by centrifugal compressors far upstream of the cascade, the cascade discharging into the test cell at atmospheric pressure.

The cascade head was manufactured from 12.5 mm perspex sheet cemented together. The end walls provided a minimum of three chord lengths of parallel passage downstream of the trailing edge. There was no control of the discharge flow in the tangential direction as this would have required very accurate a priori knowledge